# Rating of a Pitch Bearing for a 1.5-Megawatt Wind Turbine

Jonathan Keller and Yi Guo

*National Renewable Energy Laboratory*

**NREL is a national laboratory of the U.S. Department of Energy**
**Office of Energy Efficiency & Renewable Energy**
**Operated by the Alliance for Sustainable Energy, LLC**

This report is available at no cost from the National Renewable Energy Laboratory (NREL) at www.nrel.gov/publications.

Contract No. DE-AC36-08GO28308

**Technical Report**
NREL/TP-5000-82462
December 2022

# Rating of a Pitch Bearing for a 1.5-Megawatt Wind Turbine

Jonathan Keller and Yi Guo

*National Renewable Energy Laboratory*

**Suggested Citation**
Keller, Jonathan, and Yi Guo. 2022. *Rating of a Pitch Bearing for a 1.5-Megawatt Wind Turbine*. Golden, CO: National Renewable Energy Laboratory. NREL/TP-5000-82462. https://www.nrel.gov/docs/fy23osti/82462.pdf.

**NREL is a national laboratory of the U.S. Department of Energy**
**Office of Energy Efficiency & Renewable Energy**
**Operated by the Alliance for Sustainable Energy, LLC**

This report is available at no cost from the National Renewable Energy Laboratory (NREL) at www.nrel.gov/publications.

Contract No. DE-AC36-08GO28308

**Technical Report**
NREL/TP-5000-82462
December 2022

National Renewable Energy Laboratory
15013 Denver West Parkway
Golden, CO 80401
303-275-3000 • www.nrel.gov

**NOTICE**

This work was authored by the National Renewable Energy Laboratory, operated by Alliance for Sustainable Energy, LLC, for the U.S. Department of Energy (DOE) under Contract No. DE-AC36-08GO28308. Funding provided by the U.S. Department of Energy Office of Energy Efficiency and Renewable Energy Wind Energy Technologies Office. The views expressed herein do not necessarily represent the views of the DOE or the U.S. Government.



*Cover Photos by Dennis Schroeder: (clockwise, left to right) NREL 51934, NREL 45897, NREL 42160, NREL 45891, NREL 48097, NREL 46526.*

# List of Acronyms

| | |
|---|---|
| DOE | U.S. Department of Energy |
| IEC | International Electrotechnical Commission |
| ISO | International Organization for Standardization |
| kN | kilonewton |
| kNm | kilonewton meter |
| LCOE | levelized cost of energy |
| mm | millimeter |
| MPa | megapascal |
| MW | megawatt |
| m/s | meter per second |
| N | newton |
| NREL | National Renewable Energy Laboratory |
| O&M | operations and maintenance |
| OpEx | operational expenditure |
| opm | oscillations per minute |
| rpm | revolutions per minute |
| TS | technical specification |

# Table of Contents



# List of Figures



# List of Tables

# 1 Introduction

Wind power plant operational expenditures (OpEx) remain an appreciable contributor to the overall cost of wind energy, with a capacity-weighted average cost of $44 per kilowatt per year ($12 per megawatt-hour) for land-based wind plants commissioned between 2015 and 2018 in the United States (Wiser, Bolinger, and Lantz 2019). They are estimated to be up to three times that cost for offshore plants (Stehly, Beiter, and Duffy 2020). OpEx can therefore account for 25% to more than 35% of the levelized cost of energy (LCOE) of both land-based and offshore wind energy (Lantz 2013; Carroll et al. 2017; Wiser, Bolinger, and Lantz 2019). Approximately half of land-based plant OpEx are associated directly with turbine operations and maintenance (O&M) (Lantz 2013; Wiser, Bolinger, and Lantz 2019). Wind turbine O&M costs represent the single largest component of wind plant OpEx and the primary source of potential O&M cost reductions. More reliable components and better O&M strategies have the potential to reduce LCOE by 10% or more for land-based wind plants (Wiser, Bolinger, and Lantz 2019; Stehly, Beiter, and Duffy 2020) or more for fixed-bottom, offshore wind plants (Stehly, Beiter, and Duffy 2020).

Slew ring or "pitch" bearings, illustrated in Figure 1, are used in wind turbines to connect the blade root to the hub. They support the resulting simultaneous radial, axial, and overturning moment loads while allowing relative rotation of the blade with respect to the hub.

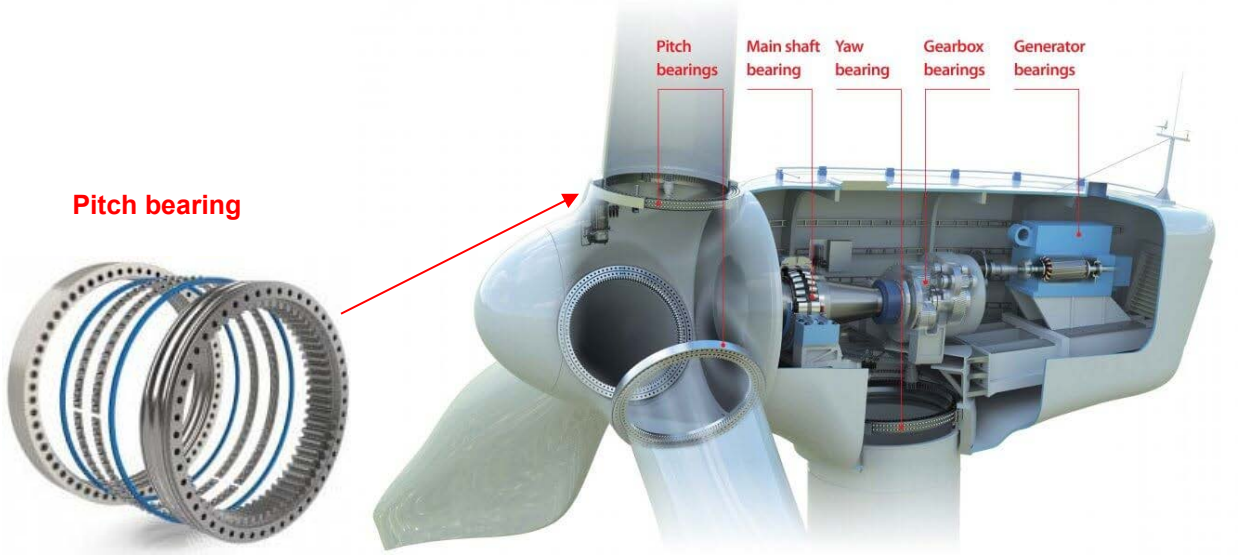


**Figure 1. Wind turbine pitch bearing (left) and nacelle (right).** ***Image from Bayles (2020)***

A common pitch bearing configuration is shown in Figure 2. The bearing consists of two rings forming the outer and inner raceways and a complement of either balls or rollers. The inner and outer rings have mounting holes that allow the bearing to be bolted directly to the supporting structures. It is common practice to cut a spur gear integral with one of the bearing rings. The balls or rollers are typically inserted into the bearing through a radial cylindrical hole in one of the rings. The hole is then closed using a removable loading plug contoured to the ball path or roller path surface. The four-point contact ball bearing type consists of a single row of balls separated by cage segments or plastic spacers. The ball groove configuration is that of a gothic arch, which provides two distinct thrust load paths for each ball. The eight-point contact ball

bearing type is similar, but it has two rows of balls in gothic arch ball grooves. The eight-point contact ball bearing type is more costly to manufacture than the single-row, four-point contact ball bearing. In addition to having a second row of balls and separators, the two-row bearing must be repeatedly assembled and disassembled during manufacture to accurately measure and match the internal diametral clearance or preload of the two ball rows (Harris, Rumbarger, and Butterfield 2009).

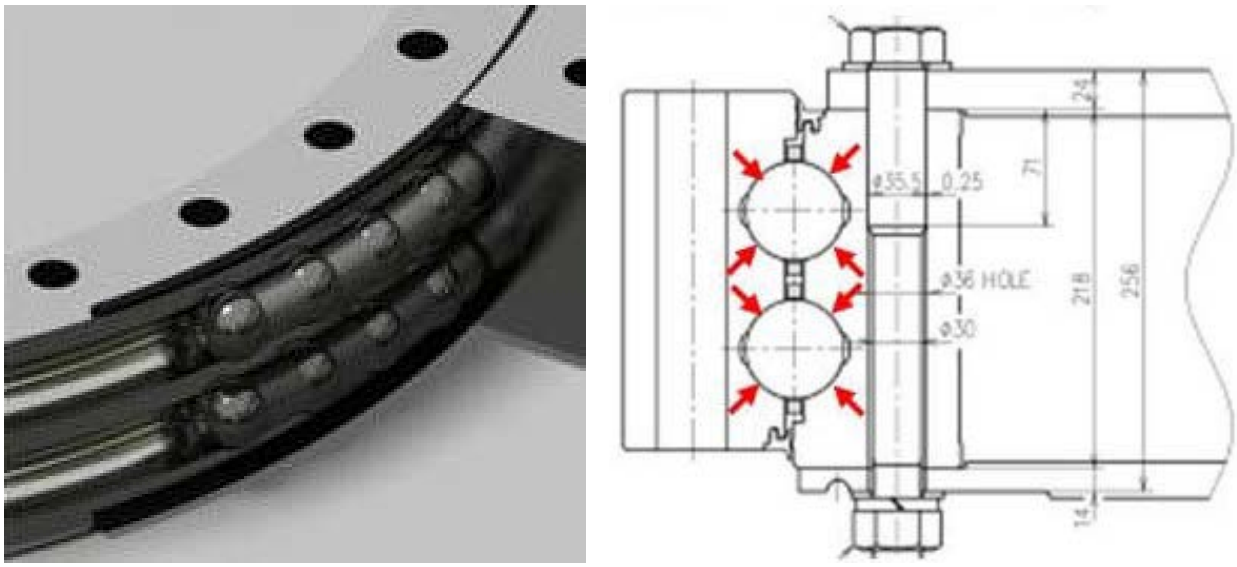


**Figure 2. Example eight-point contact ball bearing (left) and cross section (right).** ***Image from Dvorak (2016)***

## 1.1 Pitch Bearing Rating

The classic Lundberg-Palmgren theory for estimating dynamic load capacity and fatigue life for continuously rotating rolling bearings (Lundberg and Palmgren 1949) was extended for oscillating rolling bearings and correlated to laboratory fatigue life data (Rumbarger and Jones 1968), motivated by the rating of helicopter blade bearings. This included defining the critical amplitude of oscillation, the angle below which the raceway is stressed by only one roller and receives two stress repetitions per oscillation cycle because the pitch oscillation is relatively small. The calculation of the equivalent load and number of loading cycles for oscillatory applications was later presented (Houpert 1999). These formulations were then simplified and applied to wind turbine pitch bearings (Rumbarger 2003). A dither angle was defined for pitch motions even smaller than the critical amplitude, for which the stressed area is only partially uncovered and retraced. In this situation, fretting corrosion is often experienced, and the developed fatigue life models are not applicable. A similar model was also applied to a four-point contact ball bearing in a wind turbine (González et al. 2008). Additionally, the National Renewable Energy Laboratory (NREL) published a pitch and yaw bearing design guide, which summarized the design criteria, calculation methods, and applicable standards recommended for use in performance and life analyses of these bearings (Harris, Rumbarger, and Butterfield 2009). These approaches all assume purely sinusoidal oscillations. An approach for fatigue life calculation in irregularly reversing speeds and varying loads was also presented (Wöll, Jacobs, and Kramer 2018), and recently a unified calculation approach for oscillating roller bearings was also proposed (Breslau and Schlecht 2020).

The International Electrotechnical Commission (IEC) 61400-1 wind turbine design standard requires that all rolling element bearings be rated per International Organization for Standardization (ISO) 76, ISO 281, and ISO technical specification (TS) 16281. However, because pitch bearings are exposed to a discontinuous, oscillatory motion rather than a relatively constant rotation, design requirements are relatively sparse and only include that the ratio of static rating to design load is at least 1 according to ISO 76 and that the effect of flexibility on load distribution and the effect of insufficient lubrication due to small movements be considered. For pitch bearings, ISO 281 and ISO/TS 16281 are typically used to determine a modified reference (i.e., fatigue) rating life; other mechanisms of failure, like wear or microspalling, are outside their scope. ISO 281 is for bearings under continuous rotation subjected to a constant axial and/or radial load. ISO 16281 is for general loading conditions and can also account for effects of bearing-operating clearance and misalignment.

## 1.2 Pitch Bearing Reliability

Recently, there has been an increasing level of industry interest in pitch bearing reliability (Shapiro 2017; Keller et al. 2021). Some populations demonstrate a 12% failure rate in 20 years (Hornemann 2019). Although comparable information in the literature for existing offshore wind plants is sparse, it indicates that pitch system failure rates in some populations are over 2 times higher for offshore plants than land-based plants (Dao, Kazemtabrizi, and Crabtree 2019). These bearings are usually grease-lubricated, operate in boundary lubrication conditions due to their oscillating movements, are relatively susceptible to contamination, and can experience extended periods of little to no rotation (Shapiro 2017). Fatigue, wear-related failures, and frictional corrosion failures related to loading, lubrication, and sealing, which for rolling bearings are described in detail and classified in ISO 15243, have all been shown to occur (Errichello 2004; Kotzalas and Doll 2010; Dvorak 2016; Shapiro 2017; Grebe et al. 2018; Hornemann 2019; Bayles 2020; Dhanola and Garg 2020; Stammler et al. 2020; Doll 2022). Examples of macropitting and contact truncation damage on the bearing raceways are shown in Figure 3.

**Figure 3. Example pitch bearing macropitting (left, [Dvorak 2016]) and contact truncation (right, [Bayles 2020]) damage**

## 1.3 Pitch Bearing Reliability Research and Development

As rotor diameters continue to increase for tall land-based and offshore wind turbines, pitch bearings are becoming even larger in diameter, which can make them vulnerable to deflections and consequent stress concentrations. With the introduction of advanced controllers, the pitch travel characteristics of these bearings have changed. For these reasons, there is an increased need to more accurately study rolling element and raceway curvatures, deformations,

misalignment, and sliding as well as skewing, load distributions, contact stresses, edge loading, and lubrication conditions to understand pitch bearing failures.

Large-diameter pitch bearing tests have been conducted to determine friction torque (González et al. 2008; Han et al. 2015; Stammler et al. 2018; Menck et al. 2022) and fatigue lives and wear characteristics (Handreck et al. 2015; Becker et al. 2017; Grebe et al. 2018; He et al. 2018; Schwack, Prigge, and Poll 2018; Fischer and Mönnig 2019; Schwack et al. 2020; Schwack et al. 2021; Song and Karikari-Boateng 2021). Other assessments have been made of the turbine controller characteristics (Stammler, Reuter, and Poll 2018; Menck, Stammler, and Schleich 2020; Stammler et al. 2020) and stiffening plates (Loriemi et al. 2020). A model for false brinneling of cylindrical roller bearings subject to very small vibratory motions has also been proposed (Brinji, Fallahnezhad, and Meehan 2020). An updated method for determining the static load-carrying capacity of four-contact-point slewing bearings under axial, radial and tilting moment loads was also proposed (Aguirrebeitia et al. 2013).

NREL has recently begun a research program related to pitch bearing reliability, recognizing its growing importance for wind turbines. The purpose of this first paper is to describe the rating analysis for a reference pitch bearing representative of that used in a 1.5-megawatt (MW) wind turbine. The analysis will serve as a baseline for future finite-element analyses and strain and deflection measurements of an installed pitch bearing. If successful, this work will enable the design and specification of more reliable pitch bearings, a key concern in the long-term operation of land-based wind turbines and new development of offshore wind turbines.

# 2 Reference Wind Turbine and Pitch Bearing

## 2.1 Reference Wind Turbine

The U.S. Department of Energy (DOE) installed a General Electric (GE) 1.5-MW wind turbine at the NREL Flatirons Campus over the winter of 2008–2009. This turbine, hereafter referred to as the DOE 1.5, is an integral part of several research initiatives for the DOE Wind Energy Technologies Office and other industry research initiatives. The DOE 1.5 is built on the platform of the GE 1.5 SLE commercial wind turbine model but was installed in a nonstandard configuration. Important for this project and others is the fact that the DOE 1.5 is equipped with an ESS Mk 6 controller. A series of tests were previously conducted to characterize the properties and performance of the DOE 1.5, including mechanical loads per IEC 61400-11 in March 2011 (Santos and van Dam 2015). For this work, a previously developed reference model of the DOE 1.5 wind turbine was used (Shaler, Debnath, and Jonkman 2020). Relevant properties of the reference turbine model are listed in Table 1.

**Table 1. Reference Turbine Properties**

| Parameter | Value | Units[a] |
|---|---|---|
| Rated power | 1.5 | MW |
| Number of blades | 3 | - |
| Hub height | 80 | m |
| Nominal rotor diameter | 77 | m |
| Rated rotor speed | 18.3 | rpm |
| Cut-in wind speed | 3 | m/s |
| Cut-out wind speed | 25 | m/s |

[a] m = meter, m/s = meter per second, rpm = revolutions per minute

## 2.2 Reference Pitch Bearing

Several suppliers provide pitch bearings for the DOE 1.5 turbine. The description of the reference bearing in Table 2 is representative of an eight-point contact ball bearing and can be considered generally representative of the bearings currently in the market. The outer ring of the reference pitch bearing is stationary, while the inner ring rotates by an electric motor driving interior spur gear teeth. One important parameter is the critical amplitude of oscillation, $\theta_{crit}$, defined as the relative angle of rotation of the raceways for which the portion of the raceway stressed by one rolling element touches—but does not overlap—the raceway that is stressed by adjacent rollers (Rumbarger and Jones 1968).

**Table 2. Reference Pitch Bearing Properties**

| Parameter | Symbol | Value | Units[a] |
|---|---|---|---|
| Pitch diameter | $D_{pw}$ | 1,900 | mm |
| Ball diameter | $D_w$ | 34.9 | mm |
| Groove conformity (inner and outer raceways) | $f$ | 0.53 | - |
| Number of rows | $i$ | 2 | - |
| Number of rolling elements (per row) | $Z$ | 156 | - |
| Nominal contact angle | $\alpha$ | 50 | ° |
| Geometric ratio | $\gamma = D_w / D_{pw} \cos\alpha$ | 0.0118 | - |
| Critical oscillation angle (inner and outer raceways) | $\theta_{crit} = 720^\circ / Z(1 \mp \gamma)$ | 4.6 | ° |
| Core hardness | $H_B$ | 250 | - |
| Raceway surface hardness | $H_{RC}$ | 58 | - |

[a] ° = degrees, mm = millimeter

## 2.3 Reference Loads and Pitching Motion

Loads applied to the bearing are shown in Figure 4. The radial, $F_r$; thrust (or axial), $F_a$; and overturning moment, $M$, loads are shown as applied to the center of the bearing coordinate system. The magnitudes of $F_r$ and $M$ are determined from the two orthogonal components $x$ and $y$.

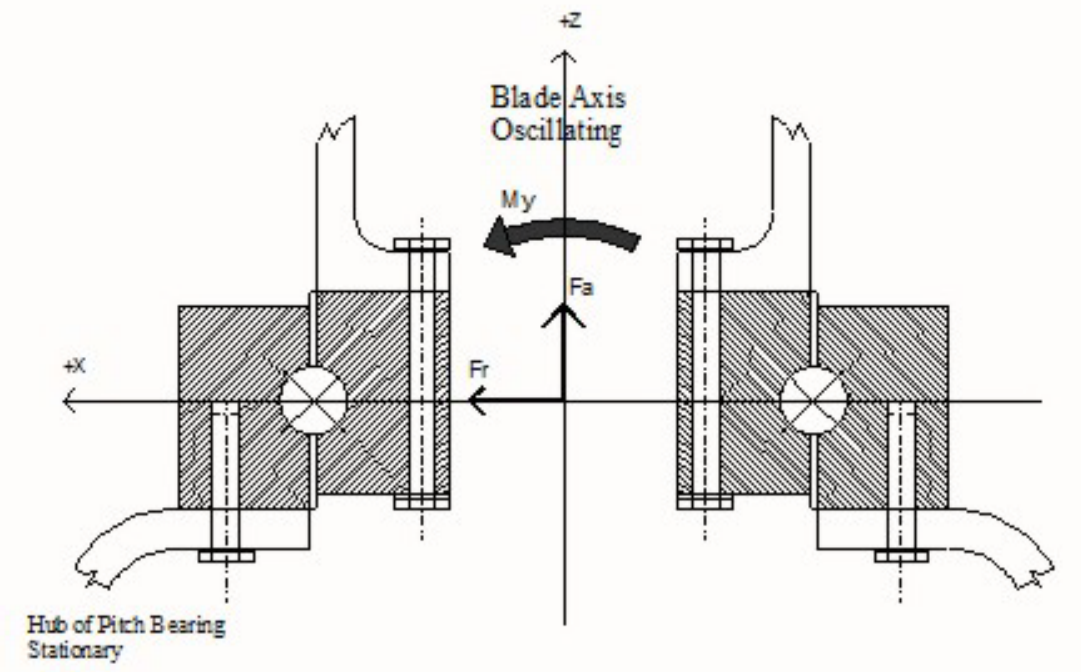


**Figure 4. Coordinate system and bearing loads.** ***Image from Harris, Rumbarger, and Butterfield (2009)***

Blade root loads and pitching motions were simulated for the reference turbine in OpenFAST version 2.2 (NREL 2022). OpenFAST is a multiphysics, multifidelity tool for simulating the dynamic response of wind turbines. It couples computational modules for aerodynamics, hydrodynamics for offshore structures (if present), control and electrical system (servo) dynamics, and structural dynamics to enable nonlinear aero-hydro-servo-elastic simulation in the time domain. Load cases were simulated for 12 different wind speeds from 3 to 25 meters per second (m/s) with a wind shear exponent of 0.2 and turbulence intensity of 0.1. A Rayleigh wind speed distribution as defined in IEC 61400-1 was assumed for the simulations. The behavior of the controller is a key characteristic of the model and can significantly influence the pitch amplitude and speed for normal load cases in response to changes in wind speed and turbulence. The reference turbine uses only collective pitch control. The duration of each simulation was 600 s, with the first 10 s being excluded from the calculation of the resulting average pitch bearing radial, axial, and moment loads. Although the rated wind speed in Table 1 is specified as 14 m/s, the simulations described here and previous modeling (Guo et al. 2021) and testing (Santos and van Dam 2015) have shown that the highest loads occur at a wind speed of approximately 11 m/s. Figure 5 shows example time histories of the resulting pitch behavior for the full 10-min. simulation and the final 10 s for reference. A 10 Hertz low-pass filter was applied to eliminate unrealistic high-speed, small-angle pitch motions. At 7 m/s, well below rated wind speed, there is almost no pitch activity even for the simulated turbulent wind conditions. However, at near- and above-rated wind conditions, the pitch activity increases as expected. At 11 m/s, the mean pitch angle is about 3° and the blade pitch oscillation (i.e., peak-to-peak) is up to 11°. As cut-out conditions are approached, the mean pitch angle increases to approximately 25° and the pitch oscillation increases to as much as 18°. These simulation results are very similar to the measured behavior in the turbine (Santos and van Dam 2015).

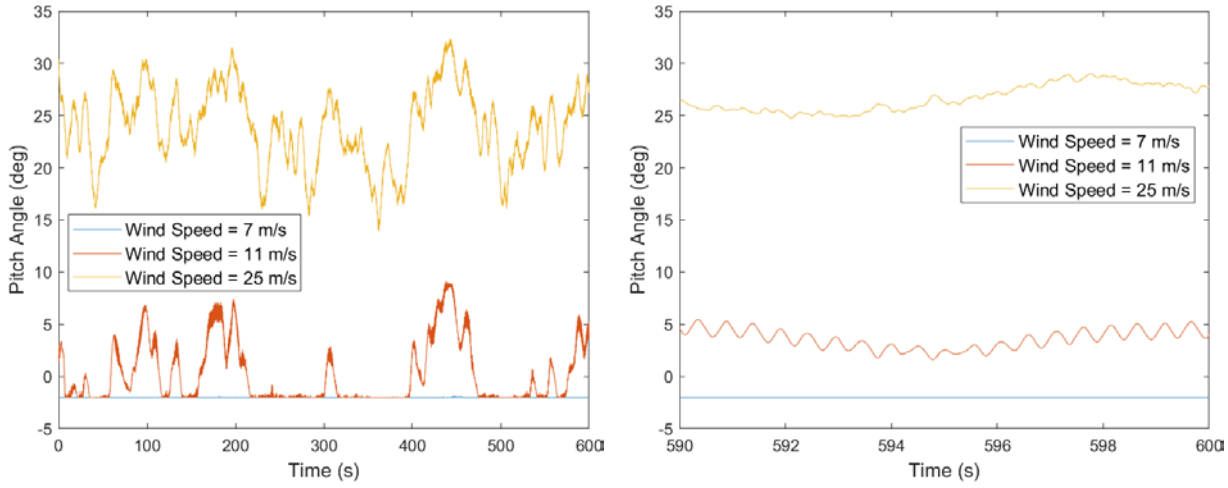


**Figure 5. Pitch time histories for the full 10-min. simulation (left) and final 10 s (right)**

To determine the oscillation angle and oscillation speed for the fatigue analysis described in the NREL design guide, rainflow cycles were counted (NREL 2022). Figure 6 shows the resulting rainflow analysis results for the 11 m/s and 25 m/s wind speed cases. In the 11 m/s case, other than the very smallest pitch movements, the most common oscillation cycle is about 1.4°, an example of which can be seen in the final 10 s of Figure 5. The resulting oscillation speed in this condition is approximately 135 oscillations per minute (opm). At 25 m/s, the smallest pitch movements dominate the cycle counting process with speeds up to 500 opm. These results are

dependent on the specifications and potential limitations for the actual pitch system. The DOE 1.5 uses an electric motor coupled to a reduction gearbox. With these results for each load case, the NREL design guide then recommends calculating a cycle-weighted average of the oscillation angle and speed. A summary of the load cases and pitching motions for the normal load cases for the reference bearing is listed in Table 3.

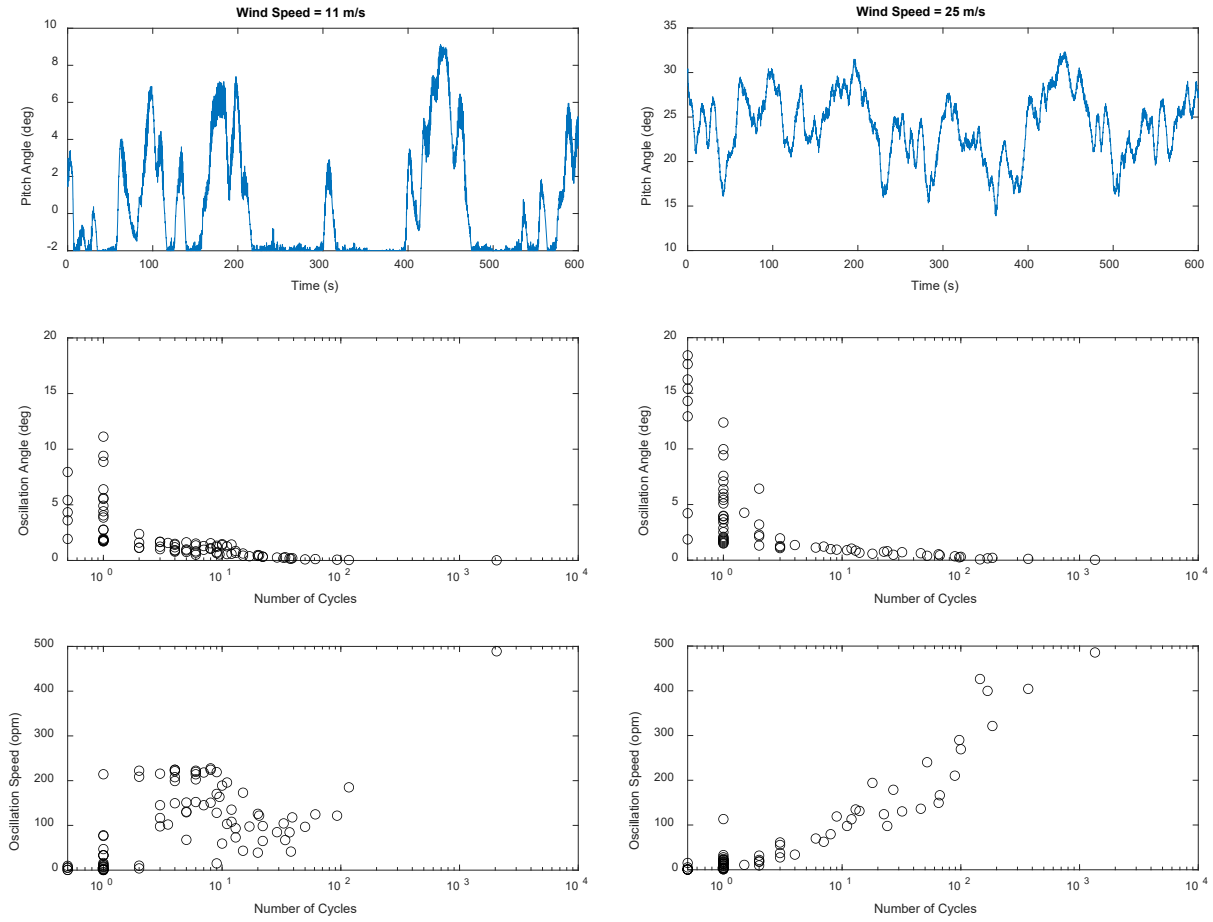


**Figure 6. Example pitch time histories, cycles, and speeds for wind speeds of 11 m/s (left) and 25 m/s (right)**

Extreme loads that can occur during faults and other situations like emergency stops are normally determined through many simulations of these individual conditions. Rather than examining all of these situations, for this analysis a safety factor of 1.35 as described in Table 3 of IEC 61400-1 was applied to the 11 m/s rated condition to estimate the extreme load components. The extreme load cases for the reference bearing are also listed in Table 3.

**Table 3. Loads and Pitching Motion**

| Load Case, $k$ | Wind Speed (m/s) | Time Share, $t$ (%) | $F_x$ (kN)[a] | $F_y$ (kN) | Radial Load, $F_r$ (kN) | Axial Load, $F_a$ (kN) | $M_x$ (kNm) | $M_y$ (kNm) | Total Moment, $M$ (kNm) | Oscillation Speed, $N$ (opm) | Oscillation Angle, $\theta$ (°) |
|---|---|---|---|---|---|---|---|---|---|---|---|
| 1 | 3 | 11.7 | 12.1 | -37.4 | 39.3 | 51.4 | 411.4 | 246.6 | 479.7 | 0 | 0 |
| 2 | 5 | 16.4 | 20.7 | -45.4 | 49.9 | 57.1 | 509.9 | 437.7 | 672.0 | 0 | 0 |
| 3 | 7 | 17.7 | 33.9 | -55.2 | 64.7 | 194.0 | 640.1 | 717.2 | 961.3 | 294.2 | 0.01 |
| 4 | 9 | 16.2 | 55.2 | -57.6 | 79.8 | 226.5 | 703.9 | 1,168.0 | 1,363.7 | 330.2 | 0.03 |
| 5 | 11 | 12.8 | 64.4 | -34.5 | 73.1 | 310.4 | 475.4 | 1,318.0 | 1,401.1 | 370.6 | 0.18 |
| 6 | 13 | 9.0 | 57.4 | -37.8 | 68.7 | 304.7 | 463.1 | 1,087.0 | 1,181.5 | 296.9 | 0.35 |
| 7 | 15 | 5.7 | 42.6 | -3.9 | 42.8 | 318.3 | 62.3 | 762.1 | 764.6 | 358.8 | 0.27 |
| 8 | 17 | 3.2 | 35.6 | -1.2 | 35.6 | 318.6 | 21.2 | 577.1 | 577.5 | 419.3 | 0.20 |
| 9 | 19 | 1.7 | 36.9 | -15.4 | 40.0 | 318.3 | 171.8 | 518.8 | 546.5 | 418.2 | 0.18 |
| 10 | 21 | 0.8 | 40.5 | -28.3 | 49.4 | 314.5 | 309.0 | 485.1 | 575.2 | 404.3 | 0.20 |
| 11 | 23 | 0.3 | 32.9 | -17.5 | 37.3 | 318.0 | 195.5 | 334.1 | 387.1 | 397.9 | 0.22 |
| 12 | 25 | 0.1 | 25.4 | -7.7 | 26.6 | 318.5 | 92.6 | 191.8 | 213.0 | 379.0 | 0.24 |
| Extreme | - | - | - | - | 98.6 | 419.0 | - | - | 1,891.5 | - | - |

[a] kN = kilonewton, kNm = kilonewton meter

# 3 Pitch Bearing Rating and Performance

This section describes the process followed in the NREL design guide to estimate the life of eight-point contact pitch bearings used in wind turbines. It also relies on associated bearing design standards such as ISO 76 and 281. In addition to static load rating and fatigue life estimation, other performance characteristics are also described.

## 3.1 Static Load Capacity

The NREL design guide uses methods related to ISO 76 to determine the static rating of pitch bearings. The static rating is related to the applied, static load resulting in permanent deformations of the rolling elements and raceways of rolling bearings. This load is associated with a total permanent deformation of 0.0001 (0.01%) of the rolling element diameter at the center of the most heavily loaded rolling element/raceway contact. Some differences in the methodologies of ISO 76 and the NREL design guide are also described.

### 3.1.1 Static Load Rating

The static load rating for the bearing can typically be obtained from a bearing manufacturer's catalog, or it can be calculated using the equations presented here and in the NREL design guide. The basic static load rating is defined in ISO 76 as the static centric load that corresponds to a calculated contact stress at the center of the most heavily loaded rolling element/raceway contact of 4,200 megapascal (MPa) for ball bearings. For this contact stress, a total permanent deformation of the rolling element and raceway occurs that would impair subsequent bearing operation. Accounting for both rows carrying axial load as in the NREL design guide, the basic static axial and radial load ratings, $C_{0a}$ and $C_{0r}$, for ball bearings are

$$\begin{aligned} C_{0a} &= f_{0a} i Z D_w^2 \sin\alpha \\ C_{0r} &= f_{0r} i Z D_w^2 \cos\alpha \end{aligned} \tag{1}$$

where the resulting values are in newtons (N) for ball diameters expressed in millimeters, and $f_{0a}$ and $f_{0r}$ are geometry factors. Using the ISO 76 method alone and based on the properties of the reference bearing, $f_{0a} \approx 60.6$ and $f_{0r} \approx 14.9$ per ISO 76; thus, $C_{0a} = 17{,}680$ kN and $C_{0r} = 3{,}650$ kN. Many slewing bearing catalogs do specify a static moment rating, but to the author's knowledge there is no publicly available method to calculate one.

Because of the multidimensional loading on the pitch bearing, the NREL design guide does not calculate the static equivalent loads and static load rating to then determine a static safety factor. Rather, it estimates the contact stress of the most heavily loaded roller and compares it to a stress limit to determine a safety factor as described in the following sections.

### 3.1.2 Static Equivalent Load

The static equivalent load is defined as the static centric load that would cause the same contact stress at the center of the most heavily loaded rolling element/raceway contact as that which occurs under the actual load conditions. Normally, for a ball bearing subjected to constant axial and radial loads, the static equivalent axial and radial load, $P_{0a}$ and $P_{0r}$, can be calculated as described in ISO 76 as the larger of the following quantities

$$P_{0a} = 2.3F_r \tan\alpha + F_a$$
$$P_{0r} = \begin{cases} X_0 F_r + Y_0 F_a \\ F_r \end{cases} \quad (2)$$

where the factors $X_0$ and $Y_0$ are static radial and axial load factors that are dependent on the contact angle and number of rows.

However, as described in Section 2.3, wind turbine pitch bearings are subjected to significant moments and widely varying axial and radial loads depending on the azimuthal position of the rotor. For this case, the NREL design guide suggests an alternate formulation. Rather than examining the static equivalent loads, it begins with a determination of the maximum rolling element load within the bearing for a given loading condition, $Q_{max}$, accounting for the combined loading

$$Q_{max} = 0.55\left(\frac{2F_r}{Z\cos\alpha} + \frac{F_a}{Z\sin\alpha} + \frac{4M}{D_{pw}Z\sin\alpha}\right) \quad (3)$$

where the factor of 0.55 (instead of 0.5) accounts for the unequal load-sharing between the two bearing rows and the units of $F_r$, $F_a$, $M$, and $D_{pw}$ must be consistent (e.g., kN, kNm, and m). Table 4 lists $Q_{max}$ for each load case for the reference bearing. The largest value for $Q_{max}$ occurs for Load Case 5 near rated conditions and for the extreme load case.

**Table 4. Maximum Rolling Element Loads**

| Load Case | Radial Load, $F_r$ (kN) | Axial Load, $F_a$ (kN) | Total Moment, $M$ (kNm) | Maximum Roller Load $Q_{max}$ (kN) |
|---|---|---|---|---|
| 1 | 39.3 | 51.4 | 479.7 | 5.3 |
| 2 | 49.9 | 57.1 | 672.0 | 7.3 |
| 3 | 64.7 | 194.0 | 961.3 | 10.9 |
| 4 | 79.8 | 226.5 | 1,363.7 | 15.1 |
| 5 | 73.1 | 310.4 | 1,401.1 | **15.8** |
| 6 | 68.7 | 304.7 | 1,181.5 | 13.6 |
| 7 | 42.8 | 318.3 | 764.6 | 9.3 |
| 8 | 35.6 | 318.6 | 577.5 | 7.5 |
| 9 | 40.0 | 318.3 | 546.5 | 7.2 |
| 10 | 49.4 | 314.5 | 575.2 | 7.6 |
| 11 | 37.3 | 318.0 | 387.1 | 5.6 |
| 12 | 26.6 | 318.5 | 213.0 | 3.8 |
| Extreme | 98.6 | 419.0 | 1,891.5 | **21.3** |

The resulting maximum stress for a point contact, $\sigma_{max}$, on the inner and outer raceway is then

$$\sigma_{\mathrm{i,o\,max}} = \frac{1.5 Q_{\max}}{\pi a_{\mathrm{i,o}} b_{\mathrm{i,o}}} \tag{4}$$

where $a$ and $b$ are the semimajor and semiminor axes of the contact ellipse. These dimensions can be determined from the dimensions of the balls and raceway grooves. For a ball bearing, the curvature sums and differences for the inner and outer raceways are

$$\sum \rho_{\mathrm{i,o}} = \frac{4}{D_{\mathrm{w}}} - \frac{1}{f_{\mathrm{i,o}} D_{\mathrm{w}}} \pm \frac{1}{D_{\mathrm{w}}} \left( \frac{2\gamma}{1 \mp \gamma} \right) \tag{5}$$

$$F(\rho)_{\mathrm{i,o}} = \frac{\frac{1}{f_{\mathrm{i,o}}} \pm \left( \frac{2\gamma}{1 \mp \gamma} \right)}{4 - \frac{1}{f_{\mathrm{i,o}}} \pm \left( \frac{2\gamma}{1 \mp \gamma} \right)} \tag{6}$$

where the upper signs refer to the inner raceway and the lower signs refer to the outer raceway. Because the reference bearing pitch diameter is large compared to the ball diameter, the curvature sums and differences for the inner and outer races are very similar. To simplify the analysis, only the inner ring values of $\Sigma\rho \approx 0.0612$/mm and $F(\rho) \approx 0.894$ are used in the remainder of the calculations. The dimensions of the contact ellipse are then

$$a_{\mathrm{i,o}} = 0.0236 a^*_{\mathrm{i,o}} \left( \frac{Q_{\max}}{\sum \rho_{\mathrm{i,o}}} \right)^{1/3} \tag{7}$$

$$b_{\mathrm{i,o}} = 0.0236 b^*_{\mathrm{i,o}} \left( \frac{Q_{\max}}{\sum \rho_{\mathrm{i,o}}} \right)^{1/3} \tag{8}$$

where in Equations (7) and (8) the curvature sum is in units of 1/mm, the maximum rolling element load, $Q_{max}$, is in units of N, and the resulting units of $a$ and $b$ are mm. The values of $a^*$ and $b^*$ are functions of $F(\rho)$ as described in the NREL design guide (Harris and Kotzalas 2007). For the reference bearing, $a^* \approx 3.0$ and $b^* \approx 0.47$. The dimensions of the contact ellipse for the two conditions of interest and resulting maximum Hertz stress per Equation (4) are listed in Table 5.

**Table 5. Maximum Hertz Stress**

| Load Case | Maximum Roller Load $Q_{max}$ (kN) | Semimajor axis of contact ellipse $a$ (mm) | Semiminor axis of contact ellipse $b$ (mm) | Maximum Hertz Stress $\sigma_{max}$ (MPa) |
|---|---|---|---|---|
| 5 | 15.8 | 4.57 | 0.70 | 2,356.6 |
| Extreme | 21.3 | 5.05 | 0.77 | 2,604.5 |

### 3.1.3 Static Safety Factor

ISO 76 defines the static safety factors as simply

$$S_0 = \frac{C_{0a}}{P_{0a}}$$
$$S_0 = \frac{C_{0r}}{P_{0r}} \quad (9)$$

and recommends a safety factor from 1 to 2, depending on the application. As stated in Section 1.1, IEC 61400-1 requires a ratio of static rating to design load of at least 1.

The NREL design guide recommends a comparison of the maximum contact stress, $\sigma_{max}$, in the limit load condition from Equation (4) to the maximum allowable stress of 4,200 MPa. It defines a similar safety factor as

$$S_0 = \left( \frac{4,200}{\sigma_{max}} \right)^3 \quad (10)$$

where the maximum contact stress, $\sigma_{max}$, is also expressed in megapascals. It recommends that the safety factor in this condition be greater than 1.5, which is the same as the ISO 76 recommendation for applications subjected to shock loads. It appears that the use of the limit load condition and a higher safety factor in the NREL design guide are stricter than the IEC 61400-1 design requirement. For the reference bearing and the loading conditions of interest listed in Table 5, the resulting static safety factor, $S_0 \approx 4.2$ in the extreme load condition and thus even higher for the normal operating conditions. No reduction in the safety factor is applied because the raceway hardness for the reference bearing is 58 $H_{RC}$, but lower hardness could be accounted for as described in the NREL design guide (Harris and Kotzalas 2007). If more extreme operating scenarios had been examined, it is likely the stresses would have been higher, resulting in a smaller static safety factor.

## 3.2 Fatigue Life

The method used in this initial analysis follows the NREL design guide for estimating rolling bearing fatigue life. It involves four major steps: calculating the dynamic load rating, the

dynamic equivalent load, and the basic rating life, and then modifying by any relevant life adjustment factors to determine the modified rating life.

### 3.2.1 Dynamic Load Rating

As described in the NREL design guide, pitch bearings are best modeled as thrust-type bearings because the principal load is an eccentrically applied thrust resulting in an axial load and an overturning moment load. The radial load affects the thrust type of load distribution but does not significantly alter it. Therefore, the fatigue life equations are based on the appropriate set of equations for an axially loaded bearing.

The basic dynamic axial load rating, $C_a$, is defined as the constant centric axial load that a rolling bearing can theoretically endure for a basic rating life of one million revolutions. For a commercial bearing, it is typically obtained from the bearing manufacturer's catalog. It can also be calculated as described in Clause 6 of ISO 281, which was selected for the purposes of illustration for the reference bearing in this study. For angular contact thrust ball bearings with ball diameters, $D_w$, greater than 25.4 mm and an identical number of rows, the basic dynamic axial load rating is

$$C_a = 3.647 b_m f_c \left(i \cos\alpha\right)^{0.7} Z^{2/3} D_w^{1.4} \tan\alpha \tag{11}$$

where the resulting value of $C_a$ is in newtons for ball diameters expressed in millimeters, $b_m$ is a rating factor depending on the bearing type and design, and $f_c$ is a geometry factor. The geometry factor $f_c \approx 42.83$. The reference bearing is assumed to include a filling slot. ISO 281 accounts for this in the rating factor for radial ball bearings in which $b_m = 1.1$, but for thrust bearings it does not and assumes $b_m = 1.3$ as has been used in some analyses (Menck, Stammler, and Schleich 2020). The basic dynamic axial load rating, $C_a$, is approximately 1,024 kN with the filling slot factor ($b_m = 1.1$) and 1,210 kN without it ($b_m = 1.3$).

In comparison, both ANSI/ABMA 9 and the NREL design guide combine the effects of $b_m$ and $f_c$ into a single factor, $f_{cm}$

$$C_a = 3.647 f_{cm} \left(i \cos\alpha\right)^{0.7} Z^{2/3} D_w^{1.4} \tan\alpha \tag{12}$$

However, there is a disparity between the values of $f_{cm}$ stated in each. The values of $f_{cm}$ in ANSI/ABMA 9 match the product of $b_m$ and $f_c$ in ISO 281 when assuming $b_m = 1.3$. The values of $f_{cm}$ in the NREL design guide only match those when including the additional factor of 1.172 for other conformity values. This document will use the ANSI/ABMA 9 convention. Based on the properties of the reference bearing, $f_{cm} \approx 55.7$; thus, $C_a = 1{,}210$ kN. This value matches the ISO 281 calculation without the filling slot factor.

The NREL design guide further modifies the basic dynamic axial load rating, $C_a$, and defines a basic dynamic axial load rating for oscillating conditions, $C_{a,osc}$. The formulation depends on a prorated angle of oscillation, $\overline{\theta}$, in comparison to the critical angle of oscillation, $\theta_{crit}$

$$C_{\mathrm{a,osc}} = \begin{cases} C_{\mathrm{a}} \left( \dfrac{180^{\circ}}{\bar{\theta}} \right)^{3/10} Z^{0.033} & \text{for } \bar{\theta} < \theta_{\mathrm{crit}} \\ C_{\mathrm{a}} \left( \dfrac{180^{\circ}}{\bar{\theta}} \right)^{1/p} & \text{for } \bar{\theta} \geq \theta_{\mathrm{crit}} \end{cases} \tag{13}$$

where the life exponent $p = 3$ for ball bearings and the prorated angle of oscillation, $\bar{\theta}$, is

$$\bar{\theta} = \frac{\sum_{k=1}^{K} N_k t_k \theta_k}{\sum_{k=1}^{N} N_k t_k} \tag{14}$$

where the load cases $k = 1 \ldots 12$ are listed in Table 3. The operational angle of oscillation is always less than the critical angle of oscillation as listed in Table 2, so for the reference bearing $C_{\mathrm{a,osc}} = 12{,}350$ kN.

### 3.2.2 Dynamic Equivalent Load

The dynamic equivalent load is defined as a constant centric (uniformly distributed) load; under the influence of this load, a rolling bearing would have the same life as it would attain under the actual load conditions. Normally, for a thrust ball bearing subjected to constant axial and radial loads, the dynamic equivalent axial load, $P_{\mathrm{a}}$, can be calculated as described in ISO 281 as

$$P_{\mathrm{a}} = XF_{\mathrm{r}} + YF_{\mathrm{a}} \tag{15}$$

where $X$ and $Y$ are dynamic radial and axial load factors that are dependent on the contact angle, number of rows, and the axial-to-radial load ratio.

However, as described in Section 2.3, wind turbine pitch bearings are subjected to significant moments and widely varying axial and radial loads depending on the rotor azimuthal position. For this case, the NREL design guide suggests an alternate formulation. It defines a different dynamic equivalent axial load, $P_{\mathrm{ea}}$, that is similar to Equation (15) but also accounts for the moment loading

$$P_{\mathrm{ea}} = 0.75F_{\mathrm{r}} + F_{\mathrm{a}} + \frac{2M}{D_{\mathrm{pw}}} \tag{16}$$

and the units of $F_{\mathrm{r}}$, $F_{\mathrm{a}}$, $M$, and $D_{\mathrm{pw}}$ must be consistent (e.g., kN, kNm, and m). It has been noted that Equation (16) yields an overestimate for the fatigue life compared to more advanced methods because the moment, $M$, represents the strongest influence on the resulting dynamic equivalent load (Menck, Stammler, and Schleich 2020). An adjustment of the last term was proposed to yield a similar life prediction as the more advanced methods

$$P_{\text{ea}} = 0.75F_{\text{r}} + F_{\text{a}} + \frac{2.5M}{D_{\text{pw}}} \tag{17}$$

The resulting dynamic equivalent axial loads for both Equations (16) and (17) are listed in Table 6. The increased contribution of the moment does have an appreciable impact on the resulting dynamic loads, in this case increasing them by approximately 15% to 20%.

**Table 6. Pitch Bearing Dynamic Equivalent Axial Loads**

| Load Case | Dynamic Equivalent Axial Load, $P_{ea}$ (Equation (16)) (kN) | Dynamic Equivalent Axial Load, $P_{ea}$ (Equation (17)) (kN) |
|---|---|---|
| 1 | 585.8 | 712.0 |
| 2 | 801.9 | 978.7 |
| 3 | 1,254.5 | 1,507.4 |
| 4 | 1,721.8 | 2,080.7 |
| 5 | 1,840.1 | 2,208.8 |
| 6 | 1,600.0 | 1,910.9 |
| 7 | 1,155.2 | 1,356.5 |
| 8 | 953.2 | 1,105.2 |
| 9 | 923.6 | 1,067.4 |
| 10 | 957.0 | 1,108.3 |
| 11 | 753.4 | 855.3 |
| 12 | 562.6 | 618.7 |

The duty cycle loading in Table 6 can be further reduced to one dynamic equivalent axial load, $\overline{P_{ea}}$, prorated for each operating condition

$$\overline{P_{\text{ea}}} = \left( \frac{\sum_{k=1}^{K} P_{\text{ea},k}^{p} N_k t_k \theta_k^x}{\sum_{k=1}^{K} N_k t_k \theta_k^x} \right)^{1/p} \qquad x = \begin{cases} 1 & \text{for } \theta_k < \theta_{\text{crit}} \\ 9/10 & \text{for } \theta_k \geq \theta_{\text{crit}} \end{cases} \tag{18}$$

where the summation is performed over the discrete number of normal load cases listed in Table 3 and depends on the angle of oscillation, $\theta$, relative to the critical angle, $\theta_{\text{crit}}$. For the given parameters of the reference bearing, $\overline{P_{ea}}$ = 1,550 kN for the NREL design guide using Equation (16) and $\overline{P_{ea}}$ = 1,853 kN using Equation (17).

### 3.2.3 Basic Rating Life

The rating life is the predicted value of life before the first evidence of fatigue develops in the material of one of the rings or one of the rolling elements. The basic rating life, $L_{10}$, is the rating life associated with 90% reliability for bearings manufactured with commonly used high-quality material, of good manufacturing quality, and operating under conventional operating conditions. Per ISO 281, it is based on the ratio of the basic dynamic load rating to the dynamic equivalent load

$$L_{10} = \left( \frac{C_{\mathrm{a}}}{P_{\mathrm{ea}}} \right)^{p} \tag{19}$$

where the resulting value of $L_{10}$ is in millions of revolutions of the bearing rings relative to each other.

It is generally agreed upon that the fatigue life of rolling element bearings subjected to cyclic oscillation, even under constant load, cannot be described adequately by the same life formulas used to describe the fatigue life of continuously rotating bearings (Harris, Rumbarger, and Butterfield 2009). The NREL design guide therefore uses the basic dynamic axial load rating for oscillating conditions to estimate the basic rating life

$$L_{10} = \left( \frac{C_{\mathrm{a,osc}}}{\overline{P_{ea}}} \right)^{p} \tag{20}$$

The NREL design guide further converts the basic rating life to a number of hours

$$L_{\mathrm{h10}} = \frac{1}{60 \sum_{k=1}^{K} N_k t_k} \left( \frac{C_{\mathrm{a,osc}}}{\overline{P_{ea}}} \right)^{p} \tag{21}$$

The basic rating life of the reference bearing is 506 million oscillations, or 37,350 hours, using $\overline{P_{ea}}$ derived from Equation (16). Because of the strong effect of the load exponent, it is only 296 million oscillations, or 21,850 hours, using $\overline{P_{ea}}$ derived from Equation (17).

### 3.2.4 Modified Rating Life

The modified rating life, $L_{\mathrm{nm}}$, is intended to account for an array of factors, such as desired reliability other than 90%, bearing fatigue load, special bearing properties, contaminated lubricant, and/or other unconventional operating conditions. In ISO 281, it is

$$L_{\mathrm{nm}} = a_1 a_{\mathrm{ISO}} L_{10} \tag{22}$$

where $a_1$ is the modification factor for reliability other than 90% and $a_{\mathrm{ISO}}$ is the modification factor for a systems approach, which accounts for a variety of other factors.

It is also common practice, such as in the NREL design guide, to define separate contributing factors for $a_{ISO}$. In this analysis

$$L_{nm} = a_1 a_2 a_3 a_4 L_{10} \tag{23}$$

The desired reliability will remain at 90% with a corresponding probability of failure, $n$ = 10%, so $a_1 = 1$. The life modification factor for material, $a_2$, for steels with a hardness less than 58 $H_{RC}$ can be estimated from

$$a_2 = \left( \frac{H_{RC}}{58} \right)^{3.6p} \tag{24}$$

Because the steel in the reference bearing is 58 $H_{RC}$, $a_2 = 1$. The life modification factor for lubrication, $a_3$, is a significant element for pitch bearings because they rotate in a slow, oscillatory fashion. If the lubricant film is sufficient to completely separate the rolling elements and raceways, fatigue life is maximized. Conversely, if the lubricant film is not of sufficient thickness to prevent contact between the rolling elements and raceways, the bearing service life is significantly reduced. For pitch bearings, the NREL design guide recommends $a_3 = 0.1$, which significantly reduces the modified rating life. Finally, the life modification factor for flexible supporting structure, $a_4$, is intended to account for the flexibility of the bearing rings and the surrounding support structure. The NREL design guide recommends $a_4 = 0.85$. Accounting for all these factors, the resulting modified rating life, $L_{10m}$, is at most 3,175 hours. The NREL design guide recommends that $L_{10m}$ be greater than 87,600 hours, which is equivalent to 50% operation over 20 years.

## 3.3 Other Performance Measures

The NREL design guide also considers other aspects of pitch bearing design and reliability. Of those, the following sections discuss subsurface shear stresses and estimated safety factors, stresses, and motions related to fretting corrosion and estimated safety factors, and finally estimated friction torque for the sizing of pitch actuators.

### 3.3.1 Case-Core Interface and Subsurface Shear Stress

The application of concentrated load by the rolling elements on the raceway results in significant subsurface shear stresses that reach down into the core material of the bearing. (Harris, Rumbarger, and Butterfield 2009). The NREL design guide defines a safety factor for subsurface shear fatigue, which is the ratio of the fatigue shear strength to stress, $\tau$, in the maximum operating condition

$$\tau = \frac{\zeta b \sum \rho}{1.8754 \cdot 10^{-5}} \tag{25}$$

where $b$ and $\sum \rho$ were previously determined in Section 3.1.2, and the resulting fatigue shear stress, $\tau$, is in megapascals. The parameter $\zeta$ and the fatigue shear strength are both interpolated from the NREL design guide. For the reference bearing, the resulting safety factor is listed in Table 7. In this case, $\tau$ does exceed the threshold, so the safety factor is less than 1.

**Table 7. Fatigue Shear Stress**

| Load Case | Seminor axis of contact ellipse $b$ (mm) | Fatigue shear stress $\tau$ (MPa) | Fatigue shear strength (MPa) | Ratio |
|---|---|---|---|---|
| 5 | 0.70 | 251.5 | 207.9 | 0.83 |

### 3.3.2 Fretting Corrosion

A fretting-corrosion type of raceway and rolling element surface failure is commonly encountered in yaw and pitch bearings. The fretting corrosion appears as elliptical or rectangular footprints at ball or roller spacing in the bearing. The markings are tiny corrosion pits caused by the lubricant being forced out of the contact area and then not being able to reenter the contact zone. The unprotected surface then is subject to corrosion pitting (Harris, Rumbarger, and Butterfield 2009).

The NREL design guide recommends stresses lower than the 4,200 MPa limit for static rating when considering fretting corrosion. These recommendations and the resulting margins of safety are listed in Table 8.

**Table 8. Fretting Corrosion Safety Factors**

| Load Case | Maximum Hertz Stress $\sigma_{max}$ (MPa) | Stress Limit (MPa) | Ratio |
|---|---|---|---|
| 5 | 2,356.6 | 2,800 | 1.19 |
| Extreme | 2,604.5 | 3,200 | 1.23 |

Another consideration for avoiding fretting corrosion is the dither angle, $\theta_{dith}$, which occurs when the pitch oscillations are small enough such that the stressed area (or footprint) between the element and the race only is partially uncovered and retraced

$$\theta_{\text{dith}} = \frac{720^{\circ} b}{\pi D_{pw}\left(1 \mp \gamma\right)} \tag{26}$$

When $\theta < \theta_{crit}/2$, it is possible for fretting corrosion to occur according to the NREL design guide. This zone would be approximately 2° for the reference bearing. When $\theta < \theta_{dith}$, fretting corrosion will most likely occur according to the NREL design guide. The dither angles in some of the previously examined cases are listed in Table 9. The oscillation angles for the lowest wind speeds are less than the dither angle, so the bearing may be susceptible to fretting corrosion in these conditions.

**Table 9. Dither Angles**

| Load Case | Semiminor axis of contact ellipse $b$ (mm) | Oscillation angle $\theta$ (°) | Dither angle $\theta_{dith}$ (°) |
|---|---|---|---|
| 1 | 0.49 | **0** | 0.06 |
| 2 | 0.54 | **0** | 0.06 |
| 3 | 0.62 | **0.01** | 0.07 |
| 4 | 0.69 | **0.03** | 0.08 |
| 5 | 0.70 | 0.18 | 0.08 |
| 6 | 0.67 | 0.35 | 0.08 |
| 7 | 0.59 | 0.27 | 0.07 |
| 8 | 0.54 | 0.20 | 0.06 |
| 9 | 0.54 | 0.18 | 0.06 |
| 10 | 0.55 | 0.20 | 0.07 |
| 11 | 0.50 | 0.22 | 0.06 |
| 12 | 0.44 | 0.24 | 0.05 |

The NREL design guide also recommends frequent (e.g., daily or after every shutdown) movement of the blade in idling conditions through an angle sufficiently large to redistribute grease to the ball groove surfaces. It suggests that this angle is greater than 3 times the critical angle of oscillation, or in the case of the reference bearing about 15°.

### 3.3.3 Friction Torque

A practical and conservative running friction torque, $T$, estimate is suggested by the NREL design guide as

$$T = \mu \frac{D_{pw}}{2}\left(\frac{4.4M}{D_{pw}} + 2.2F_r + F_a\right) \tag{27}$$

where the coefficient of friction, $\mu$, is approximately $\mu \approx 0.004$. The estimated running friction torque for the two highest load cases is listed in Table 10.

**Table 10. Friction Torque**

| Load Case | Radial Load, $F_r$ (kN) | Axial Load, $F_a$ (kN) | Total Moment, $M$ (kNm) | Friction Torque $T$ (kNm) |
|---|---|---|---|---|
| 5 | 73.1 | 310.4 | 1,318.0 | 14.1 |
| Extreme | 98.6 | 419.0 | 1,891.5 | 19.0 |

# 4 Conclusions

NREL has recently begun a research program related to pitch bearing reliability, recognizing its growing importance as land-based wind turbines continue to age and larger, offshore wind turbines are developed and installed. In this paper, a rating and performance analysis of a reference pitch bearing for a 1.5-MW wind turbine was conducted in accordance with the NREL pitch and yaw bearing design guide. Bearing loading was determined from an OpenFAST model of the reference turbine. The analysis is intended to serve as a baseline for future finite-element analyses and strain and deflection measurements of a pitch bearing installed in the DOE 1.5 turbine at the NREL Flatirons Campus.

Key conclusions from the rating and performance analysis are:

- The static safety factor is 4.2, calculated by comparing the maximum ball-to-raceway contact stress to the stress limit specified in ISO 76. This is greater than the requirement of 1.0 for the ratio of static rating to design load specified in IEC 61400-1.
- The basic rating life, which is the rating life associated with 90% reliability before the first evidence of fatigue develops, is estimated to be between 21,850 and 37,350 hours depending on the weighting factors applied to the axial, radial, and moment loads.
- The modified rating life, which is intended to account for a variety of application-specific factors, is estimated to be approximately 3,175 hours. This reduction to less than 10% of the basic rating life is driven primarily by the assumed life modification factor for lubrication related to slow-speed, oscillatory motion and dominates the rating life calculation. This represents a large design uncertainty that can easily result in an over or underdesigned bearing, and merits further research.
- The estimated safety factor is less than 1 related to subsurface shear stress and greater than 1 related to fretting corrosion.

This analysis simplifies calculation of the dynamic equivalent axial load. The NREL design guide and ISO 16281 describe more detailed formulations of the load distribution among the rollers, which depend on the operating clearance and preload, the bearing stiffness, and other detailed design parameters in each row and between rows. Future work will consider these effects, especially when compared to the planned strain and deflection measurements. Finally, pitch bearing rating for larger reference wind turbines, representative of those used offshore, will also be undertaken in the future.

# References


Aguirrebeitia, J., J. Plaza, M. Abasolo, and J. Vallejo. 2013. "General Static Load-Carrying Capacity of Four-Contact-Point Slewing Bearings for Wind Turbine Generator Actuation Systems." *Wind Energy* 16(5): 759–774. doi: 10.1002/we.1530.

Bayles, C. 2020. "Extending Wind Turbine Life With Pitch Bearing Upgrades." *Windpower Engineering & Development* 12(1): 16–20. https://www.windpowerengineering.com/extending-wind-turbine-life-with-pitch-bearing-upgrades/.

Becker, D., A. Gockel, T. Handreck, B. Lüneburg, T. Netz, and G. Volmer. 2017. "State-of-the-art design process for pitch bearing applications of multi-MW wind turbine generators." Presented at Conference for Wind Power Drives 2017.

Breslau, G. and B. Schlecht. 2020. "A Fatigue Life Model for Roller Bearings in Oscillatory Applications." *Bearing World Journal* 5: 65–80. https://www.vdma-verlag.com/home/download_10681.html.

Brinji, O., K. Fallahnezhad, and P.A. Meehan. 2020. "Analytical Model for Predicting False Brinelling in Bearings." *Wear* 444–445: 203135. doi: 10.1016/j.wear.2019.203135.

Carroll, J., A. McDonald, I. Dinwoodie, D. McMillan, M. Revie, and I. Lazakis. 2017. "Availability, Operation and Maintenance Costs of Offshore Wind Turbines with Different Drive Train Configurations." *Wind Energy* 20(2): 361–378. doi: 10.1002/we.2011.

Dao, C., B. Kazemtabrizi, and C. Crabtree. 2019. "Wind Turbine Reliability Data Review and Impacts on Levelised Cost of Energy." *Wind Energy* 22(12): 1848–1871. https://doi.org/10.1002/we.2404.

Dhanola, A. and H.C. Garg. 2020. "Tribological Challenges and Advancements in Wind Turbine Bearings: A Review." *Engineering Failure Analysis* 118: 104885. doi: 10.1016/j.engfailanal.2020.104885.

Doll, G.L. 2022. "Surface Engineering in Wind Turbine Tribology." *Surface and Coatings Technology*, 442: 128545. doi: 10.1016/j.surfcoat.2022.128545.

Dvorak, P. 2016. "Making Short Lived Pitch Bearing Work Longer." *Windpower Engineering & Development*. https://www.windpowerengineering.com/making-short-lived-pitch-bearing-work-longer/.

Errichello, R. 2004. "Another Perspective: False Brinelling and Fretting Corrosion." *Tribology & Lubrication Technology* 60(4): 34–36.

Fischer, J. and P. Mönnig. 2019. "Challenges for the Design Process of Pitch Bearings and the Contribution of Test Benches." Presented at Conference for Wind Power Drives 2019.

González, J.P., F.J. Echarte Casquero, J. Vázquez Mato, and M.A. González-Posada. 2008. "Blade Bearing Friction and Fatigue Mathematical Mode." Proceedings of the STLE/ASME 2008 International Joint Tribology Conference. STLE/ASME 2008 International Joint Tribology Conference. Miami, Florida, USA. October 20–22, 2008. pp. 427–431. ASME. doi: 10.1115/IJTC2008-71147.

Grebe, M., J. Molter, F. Schwack, and G. Poll. 2018. "Damage Mechanisms in Pivoting Rolling Bearings and Their Differentiation and Simulation." *Bearing World Journal* 3: 71–86. http://kth.diva-portal.org/smash/record.jsf?pid=diva2%3A1433594&dswid=6752.

Guo, Y., O. Bankestrom, R. Bergua, J. Keller, and M. Dunn. 2021. "Investigation of Main Bearing Operating Conditions in a Three-Point Mount Wind Turbine Drivetrain." *Forschung im Ingenieurwesen* 85: 405–415. doi: 10.1007/s10010-021-00477-8.

Han, J.W., J.S. Nam, Y.J. Park, G.H. Lee, and Y.Y. Nam. 2015. "An Experimental Study on the Performance and Fatigue Life of Pitch Bearing for Wind Turbine." *Journal of Mechanical Science Technology* 29(5): 1963–1971. doi: 10.1007/s12206-015-0417-2.

Handreck, T., D. Becker, J. Rollmann, B. Lüneburg. 2015. "Determining the Characteristics of Large Diameter Ball and Roller Bearings." Presented at Conference for Wind Power Drives 2015.

Harris, T.A. and M.N. Kotzalas. 2007. *Rolling Bearing Analysis, 5th Edition*. London: Taylor and Francis Group, CRC Press.

Harris, T., J.H. Rumbarger, and C.P. Butterfield. 2009. *Wind Turbine Design Guideline DG03: Yaw and Pitch Rolling Bearing Life*. Golden, CO: National Renewable Energy Laboratory. NREL/TP-500-42362. https://www.nrel.gov/docs/fy10osti/42362.pdf.

He, P., R. Hong, H. Wang, and C. Lu. 2018. "Fatigue Life Analysis of Slewing Bearings in Wind Turbines." *International Journal of Fatigue* 111: 233–242. doi: 10.1016/j.ijfatigue.2018.02.024.

Hornemann, M. 2019. "Top Failure Observations from the Field." Presented at Drivetrain Reliability Collaborative Meeting, February 20, 2019. https://app.box.com/s/7vo2ssy085raoeqa8wnyh5lrfjne6lgs.

Houpert, L. 1999. "Bearing Life Calculation in Oscillatory Applications." *Tribology Transactions* 42(1): 136–143. doi: 10.1080/10402009908982200.

Keller, J., S. Sheng, Y. Guo, B. Gould, and A. Greco. 2021. *Wind Turbine Drivetrain Reliability and Wind Plant Operations and Maintenance Research and Development Opportunities*. Golden, CO: National Renewable Energy Laboratory. NREL/TP-5000-80195. http://www.nrel.gov/docs/fy21osti/80195.pdf.

Kotzalas, M.N. and G.L. Doll. 2010. "Tribological Advancements for Reliable Wind Turbine Performance." *Philosophical Transactions of the Royal Society A* 368: 4829–4850. doi: 10.1098/rsta.2010.0194.

Lantz, E. 2013. *Operations Expenditures: Historical Trends and Continuing Challenges* (Presentation). Golden, CO: National Renewable Energy Laboratory. NREL/TP-5000-58606. http://www.nrel.gov/docs/fy13osti/58606.pdf.

Loriemi, A., G. Jacobs, D. Bosse, and M. Zweiffel. 2020. "Improvement of the Pitch Bearing Load Distribution by Shape-Optimized Stiffening Plates." *Journal of Physics: Conference Series* 1618: 052025. doi: 10.1088/1742-6596/1618/5/052025.

Lundberg, G. and A. Palmgren. 1949. "Dynamic Capacity of Rolling Bearings." *Journal of Applied Mechanics* 16(2): 165–172. doi: 10.1115/1.4009930.

Menck, O., M. Stammler, and F. Schleich. 2020. "Fatigue Lifetime Calculation of Wind Turbine Blade Bearings Considering Blade-Dependent Load Distribution." *Wind Energy Science* 5: 1743–1754. doi: 10.5194/wes-5-1743-2020.

Menck, O., K. Behnke, M. Stammler, A. Bartschat, F. Schleich, and M. Graßmann. 2022. "Measurements and Modeling of Friction Torque of Wind Turbine Blade Bearings." *Journal of Physics: Conference Series* 2265: 022087. doi 10.1088/1742-6596/2265/2/022087.

National Renewable Energy Laboratory (NREL). 2022. "OpenFAST Documentation." Accessed 6 April 2022. https://openfast.readthedocs.io/.

Rumbarger, J. H. and A. B. Jones. 1968. "Dynamic Capacity of Oscillating Rolling Element Bearings." *Journal of Lubrication Technology* 90(1): 130–138. doi: 10.1115/1.3601528.

Rumbarger, J. H. 2003. "Simplification of Dynamic Capacity and Fatigue Life Estimations for Oscillating Rolling Bearings." *Journal of Tribology* 125(4): 868–870. doi: 10.1115/1.1576424.

Santos, R. and J. van Dam. 2015. *Mechanical Loads Test Report for the U.S. Department of Energy 1.5-Megawatt Wind Turbine*. Golden, CO: National Renewable Energy Laboratory. NREL/TP-5000-63679. http://www.nrel.gov/docs/fy15osti/63679.pdf.

Schwack, F., F. Prigge, and G. Poll. 2018. "Finite Element Simulation and Experimental Analysis of False Brinelling and Fretting Corrosion." *Tribology International* 126: 352–362. doi: 10.1016/j.triboint.2018.05.013.

Schwack, F., N. Bader, J. Leckner, C. Demaille, and G. Poll. 2020. "A Study of Grease Lubricants Under Wind Turbine Pitch Bearing Conditions." *Wear* 454–455: 203335. doi: 10.1016/j.wear.2020.203335.

Schwack, F., F. Halmos, M. Stammler, G. Poll, S. Glavatskih. 2021. "Wear in Wind Turbine Pitch Bearings—A Comparative Design Study." *Wind Energy* 25(4): 700–718. doi: 10.1002/we.2693.

Shaler, K., M. Debnath, and J. Jonkman. 2020. "Validation of FAST.Farm Against Full-Scale Turbine SCADA Data for a Small Wind Farm". *Journal of Physics: Conference Series* 1618: 062061. doi: 10.1088/1742-6596/1618/6/062061.

Shapiro, M. 2017. "Pitch Bearing Investigations." Presented at Drivetrain Reliability Collaborative Meeting, February 21, 2017. https://app.box.com/s/tgv9r5vpwslex2f4uh5ssk1qtwev0bxq.

Song, W. and A. K. Karikari-Boateng. 2021. "Enhanced Test Strategy of Pitch Bearing Based on Detailed Motion Profile." Presented at Conference for Wind Power Drives 2021.

Stammler, M., A. Reuter, and G. Poll. 2018. "Cycle Counting of Roller Bearing Oscillations – Case Study of Wind Turbine Individual Pitching System." *Renewable Energy Focus* 25: 40–47. doi: 10.1016/j.ref.2018.02.004.

Stammler, M., F. Schwack, N. Bader, A. Reuter, and G. Poll. 2018. "Friction Torque of Wind-Turbine Pitch Bearings – Comparison of Experimental Results With Available Models." *Wind Energy Science* 3: 97–105. doi: 10.5194/wes-3-97-2018.

Stammler, M., P. Thomas, A. Reuter, F. Schwack, and G. Poll. 2020. "Effect of Load Reduction Mechanisms on Loads and Blade Bearing Movements of Wind Turbines." *Wind Energy* 23(2): 274–290. doi: 10.1002/we.2428.

Stehly, T., P. Beiter, and P. Duffy. 2020. *2019 Cost of Wind Energy Review*. Golden, CO: National Renewable Energy Laboratory. NREL/TP-5000-78471. https://www.nrel.gov/docs/fy21osti/78471.pdf.

Wiser, R., M. Bolinger, and E. Lantz. 2019. "Assessing Wind Power Operating Costs in the United States: Results from a Survey of Wind Industry Experts." *Renewable Energy Focus* 30: 46–57. doi: 10.1016/j.ref.2019.05.003.

Wöll, L., G. Jacobs, and A. Kramer. 2018. "Lifetime Calculation of Irregularly Oscillating Bearings in Offshore Winches." *Modeling, Identification and Control* 39(2): 61–72. doi: 10.4173/mic.2018.2.2.